

Nitrogen Plasma Passivated Niobium Resonators for Superconducting Quantum Circuits

K. Zheng,¹ D. Kowsari,¹ N. J. Thobaben,² X. Du,¹ X. Song,¹ S. Ran,¹ E. A. Henriksen,^{1,3} D. S. Wisbey,² and K. W. Murch¹

¹*Department of Physics, Washington University, Saint Louis, Missouri, 63130, USA*

²*Department of Physics, Saint Louis University, Saint Louis, Missouri, 63103, USA*

³*Institute of Materials Science and Engineering, Washington University, Saint Louis, Missouri, 63130, USA*

(*Email address: murch@physics.wustl.edu)

(Dated: 4 June 2022)

Microwave loss in niobium metallic structures used for superconducting quantum circuits is limited by a native surface oxide layer formed over a timescale of minutes when exposed to an ambient environment. In this work, we show that nitrogen plasma treatment forms a niobium nitride layer at the metal-air interface which prevents such oxidation. X-ray photoelectron spectroscopy confirms the doping of nitrogen more than 5 nm into the surface and a suppressed oxygen presence. This passivation remains stable after aging for 15 days in an ambient environment. Cryogenic microwave characterization shows an average filling factor adjusted two-level-system loss tangent $F\delta_{\text{TLS}}$ of $(2.9 \pm 0.5) \cdot 10^{-7}$ for resonators with 3 μm center strip and $(1.0 \pm 0.3) \cdot 10^{-7}$ for 20 μm center strip, exceeding the performance of unpassivated samples by a factor of four.

Increasing the coherence time of superconducting qubits while maintaining reasonable gate speeds enables more powerful quantum processors^{1,2}. The improvement of fabrication techniques plays an important role in this effort^{3,4}. The fabrication process of high coherence planar superconducting quantum processors now typically involves two superconducting layers. The first layer makes up the ground plane and all the circuit elements other than the Josephson junction^{5,6} (JJ) while the second layer defines the JJs. The two-layer process allows optimization of the quality factor of the superconducting capacitor pads independent from the requirements of the double-angle-evaporated aluminum JJ layer. Microwave coplanar waveguide (CPW) resonators have been demonstrated as a robust platform to characterize the microwave loss in superconducting materials^{7,8}, and have been instrumental in the continuous improvement of film and device quality^{9,10}. The microwave loss of state-of-the-art superconducting materials at low excitation powers is ultimately limited by two-level-system (TLS) defects that primarily reside at the metal-air (MA), metal-substrate (MS), and substrate-air (SA) interfaces¹¹. For Nb resonators, most of the TLSs reside in the oxide layer at the MA interface and the removal of the oxide¹² produces CPW resonators with single-photon internal quality factor Q_i up to 5 million and filling factor adjusted two-level-system loss tangent $F\delta_{\text{TLS}}$ down to $9 \cdot 10^{-8}$. However, the oxide grows back following a Cabrera-Mott¹³ behavior within several hours, reintroducing TLSs at the MA interface^{14,15} (Fig. 1). As the buffered oxide etch (BOE) used to etch NbO_x also etches the Al JJ¹⁶, it is difficult to incorporate Nb resonators with a low density of TLSs at the MA interface into superconducting quantum circuits.

Nitride superconductors such as NbN and TiN are known to only have a thin native surface oxide layer at room temperature and therefore are expected to have fewer TLSs at the MA interface¹⁷. However, it is suspected that the reactive sputtering process required to produce high quality nitride films forms a SiN_x layer at the MS interface¹⁸ which introduces additional TLSs compared to elemental superconductors¹⁹. If a

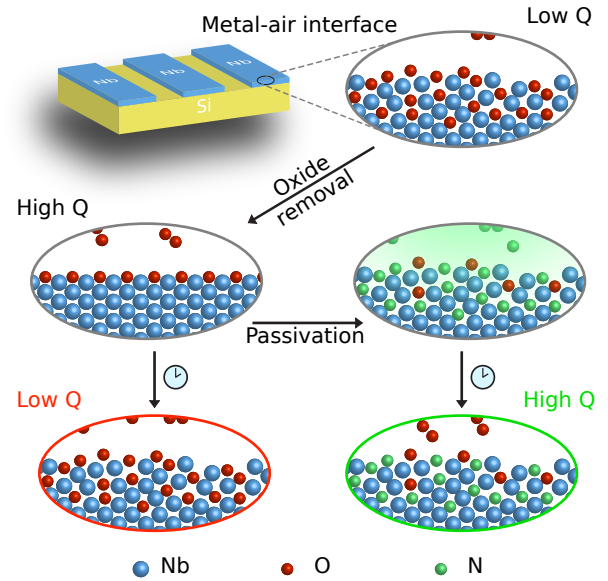


FIG. 1. Nitrogen passivation of Nb resonators. Nb films grow an amorphous oxide layer at the MA interface that results in low quality factor. Removal of this oxide with a BOE clean improves Q , but the oxide regrows over time (left). Passivating the MA interface with N inhibits the growth of oxides, maintaining high Q over time.

resonator could have the MA interface from a nitride superconductor and the MS interface from an elemental superconductor, then its microwave loss caused by TLS is expected to be extremely low. There have been attempts to deposit a thin TiN film covering Nb to prevent the growth of NbO_x ²⁰, but the sidewalls are not covered by TiN and can still oxidize.

Nitrogen doping²¹ is a well-established technique used to create low-loss Nb 3D cavities. By baking the Nb cavity in N_2 gas at a temperature above 800 $^\circ\text{C}$, a conformal layer of NbN_x is formed at the MA interface which inhibits the growth of surface oxide²². In theory, this method can be adapted to

make planar superconducting devices, however the effect of high temperature is not yet well understood. Treatment at high temperature can change the stress and grain size of the deposited metal and allow Nb to diffuse into a substitutional site inside the Si substrate, which all could potentially affect microwave loss^{23–25}. Baking at high temperature can also introduce dislocation and vacancy defects in the Si substrate, whose effects on microwave loss have not yet been systematically explored.

In this Letter, we demonstrate nitrogen doping of Nb CPW resonators without introducing potentially performance-limiting defects related to high temperature. We utilize a radio frequency (RF) plasma to satisfy the activation energy required for nitrogen doping. We show that a N_2 plasma at 300 °C for 10 minutes dopes the top 5 nm of the Nb surface with N which suppresses the growth of Nb oxides at the surface. Furthermore, we demonstrate that the passivation remains robust in an ambient air environment for sufficiently long periods of time to incorporate passivated Nb structures into complex, multi-layer quantum processors. Our process can be easily manifested with equipment available in typical industrial and academic facilities.

The films used in this study are fabricated by first cleaning a 2-inch intrinsic Si (111) wafer²⁶ with resistivity greater than 8000 $\Omega\cdot\text{cm}$ in piranha solution (3:1 mixture of H_2SO_4 and H_2O_2) at 120 °C for 10 minutes followed by a BOE clean (7:1 mixture of NH_4F and HF) for 5 minutes. We then load the wafer into an electron-beam evaporation chamber (AJA ATC-ORION-8E) in less than 3 minutes. We evaporate 250 nm of Nb (99.95% purity) at a chamber pressure of $3 \cdot 10^{-9}$ Torr and a rate of 2 nm/min at room temperature.

The resonator pattern is defined after we deposit the Nb film and before the passivation steps. We utilize a positive photoresist (MicroChem Shipley S1805) and a 375 nm optical direct-write laser lithography system (Heidelberg DWL 66+) to pattern the film. We etch the patterned film using a mixture of SF_6 and Ar in an RIE system (Oxford Plasma Lab 100 ICP). Our etching recipe produces a ~ 400 nm deep trench in the Si substrate. We then oxygen plasma ash the samples (100 W, 15 sccm O_2) for 30 s and finally soak them in MicroChem Remover PG for > 8 hrs at 70 °C to remove the remaining resist.

To passivate the samples, we start by performing a BOE clean for 30 minutes to remove all the surface oxide before transferring the wafer into a plasma enhanced chemical vapor deposition (PECVD) chamber (Oxford Instruments Nanofab). The transfer time between removal from the BOE solution and evacuation of the PECVD chamber is kept below 3 minutes. We first let the wafer sit at 300 °C for 10 minutes with 1200 sccm N_2 flow and a chamber pressure of 1 Torr. We then start a 20 W RF plasma at the same chamber condition for 10 minutes. Lastly, we cool down the chamber to 100 °C with 100 sccm of N_2 flow over the course of one hour before removing the sample. We perform a third BOE clean for 15 s to remove the thin SiN_x layer on the exposed Si substrate in the trenches.

The PECVD system uses a routine process to remove oxides from the chamber walls. This process introduces residual

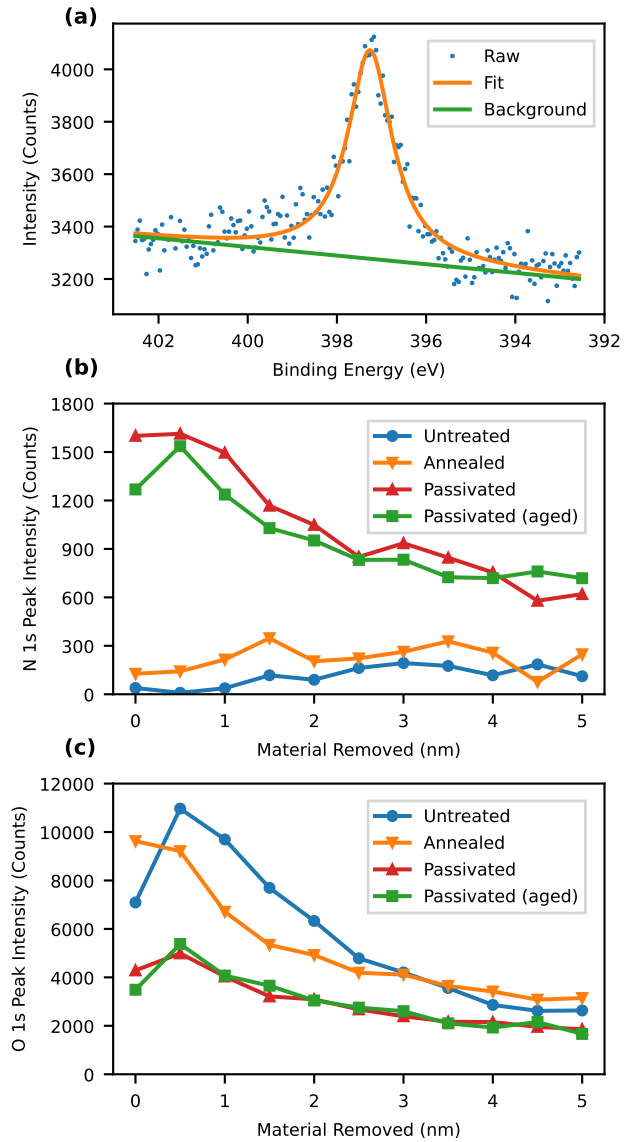


FIG. 2. XPS depth profile of N and O on Nb surfaces with different treatments. (a) The observed N 1s peak for a passivated Nb film at 1 nm depth. (b, c) The N 1s peak (b) and the O 1s peak (c) for different film treatments as a function of etch depth by in-situ Ar ion milling.

F in the chamber which reacts with the Nb films. To mitigate contamination from F, we deposit $\sim 1 \mu\text{m}$ of SiO_x on a dummy wafer and the chamber wall immediately before passivating our sample.

We characterize the surface atomic species of passivated and unpassivated Nb films using X-ray Photoelectron Spectroscopy (XPS). The XPS system (Physical Electronics 5000 VersaProbe II Scanning ESCA Microprobe) uses an Al K_{α} line source and in-situ Ar ion milling to facilitate analysis of material at depth. Figure 2(a) shows the XPS scan of a passivated Nb film with its top 1 nm removed. The observed peak corresponds to N 1s electrons. We fit the N 1s peak to a pseudo-Voigt function and the background to a linear func-

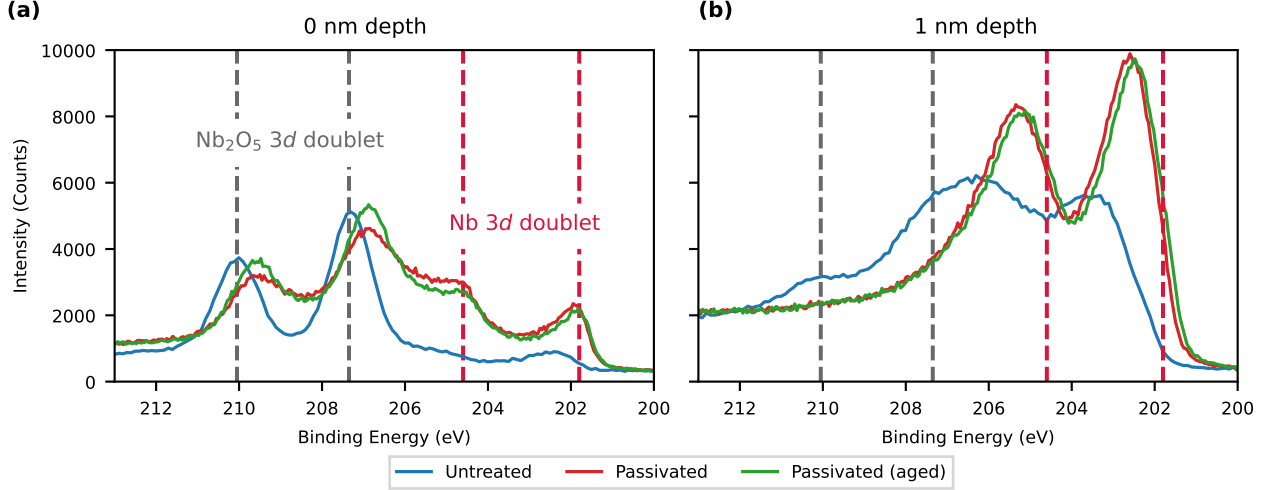


FIG. 3. XPS spectrum of the Nb 3d peaks with (a) 0 nm, and (b) 1 nm of surface material removed.

tion. We use the same practice to fit all the N 1s and O 1s²⁷ peaks measured in this study.

Figure 2(b) shows the area under the N 1s peak as a function of surface material removed for Nb films with different treatments. The untreated sample and the sample that is simply annealed in N₂ at 300 °C without lighting a plasma do not show a strong N presence. In comparison, plasma passivated Nb film shows a well-defined N peak that persists to a depth of 5 nm, which suggests successful incorporation of N atoms. The intensity of the N peak does not change significantly after we age the passivated Nb sample in an ambient environment for 15 days. In Fig. 2(c), we show that the presence of O in the surface 5 nm is reduced for passivated samples. Similar to N, the O concentration in the plasma passivated sample does not change after being aged in an ambient environment for 15 days.

The study of N and O 1s electrons confirms a suppressed oxygen concentration near the surface for passivated samples. We now examine the Nb 3d electrons to investigate the oxides present near the surface of the films. Figure 3 shows the raw XPS spectrum of the different chemical states of the Nb 3d peaks from the same samples shown in Fig. 2. As the stoichiometry of the oxide layer is complex²⁸ and we have also introduced a nitride with unknown stoichiometry, we expect the spectrum to contain at least 10 individual peaks that overlap with each other. We examine the trend of two sets of easily defined peaks. At zero depth [Fig. 3(a)] we observe clear Nb 3d doublet peaks corresponding to Nb₂O₅ for the unpassivated films. The passivated films do not exhibit these clear peaks (corresponding to O-rich oxides), rather there is a larger weight at smaller binding energy, corresponding to Nb of lower valency states. As shown in Fig. 3(b), at 1 nm depth the unpassivated samples still exhibit significant intensity at the Nb₂O₅ doublet energies. In contrast, the passivated sample shows intensity primarily at the Nb 3d doublet peaks. We

also observe that the passivated sample does not accumulate more oxide at the surface after being aged for 15 days.

To study the effect of the passivation process on the quality of the Nb films, we measure the direct-current (DC) resistance of the passivated and the untreated films as a function of temperature using a 4-point technique inside a Quantum Design physical property measurement system (PPMS). Both samples are diced from the same Nb film deposited on the same Si (111) wafer allowing us to attribute the change in film properties to the passivation process alone. We extract the residual resistivity ratio (RRR) by taking the ratio between the resistance value at 297 K and 10 K. We find that the untreated sample has a RRR of 4.86, which is similar to our previous result on Si (100)²⁹. The plasma passivated sample has a reduced RRR value of 2.96. Figure 4(a) shows the resistance near the superconducting transition of both samples. We observe a superconducting critical temperature T_c of 9.28 ± 0.05 K for the untreated sample, and a suppressed T_c of 8.49 ± 0.05 K for the plasma passivated sample with T_c taken from the temperature value when the resistance drops to half of its residual value in the normal state. Figure 4(b) shows the X-ray diffraction (XRD) spectrum of both samples measured in a Rigaku MiniFlex system with a Cu K α source. Although both samples show similar texture, the Nb (110) peak of the passivated sample has about half of the intensity compared to the untreated film. Both the resistance and the XRD measurements show that our passivation process produces a more disordered superconductor.

We utilize cryogenic microwave measurements to extract the power-dependent quality factor of CPW resonator structures, and to study the effect of passivation on the TLS-induced loss in the devices. We apply the passivation process to the resonators after the CPW structures are defined with RIE so that the sidewalls of the resonators are also passivated. The resonators are capacitively coupled to a transmission line

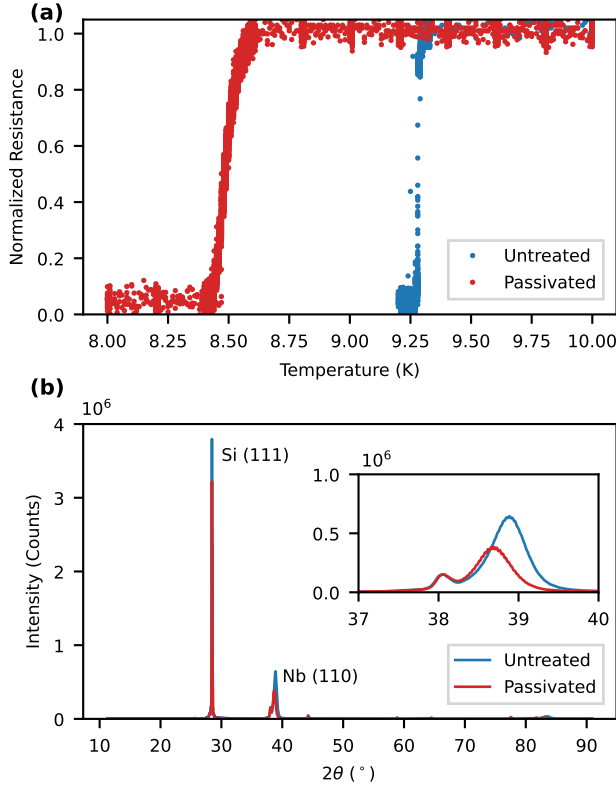


FIG. 4. (a) Superconducting transition of plasma passivated and untreated samples. (b) XRD 2θ scan of plasma passivated and untreated Nb films. The inset shows the Nb (110) peaks from Cu $K_{\alpha 1}$ and $K_{\alpha 2}$.

with coupling quality factor $Q_c \simeq 0.5 \times 10^6$. Hanger-style resonators^{29,30} with two types of geometries are fabricated. The first geometry has a center strip width of $3 \mu\text{m}$, gap width of $2 \mu\text{m}$, and has a continuous ground plane. This design allows us to clearly observe the effect of TLSs by maximizing capacitive dielectric loss¹¹ and minimizing inductive^{31,32} and radiative³³ losses. The second geometry has center strip width of $20 \mu\text{m}$, gap width of $12 \mu\text{m}$, and has holes ($5 \times 5 \mu\text{m}^2$ squares) periodically (every $15 \mu\text{m}$) etched into the ground plane³⁴. This design minimizes the capacitive loss but is more susceptible to radiative loss³³ and loss caused by trapped magnetic flux³¹. We use GE varnish to attach each resonator sample to a microstrip-style microwave launch with Pd-coated Cu metallization and Rogers Duroid 6010LM dielectric. We make 3 wirebonds to each port with 1 mil Al-1%Si bonding wire. The microstrip launch is enclosed inside a Pd-coated Cu sample package. The package is cooled inside a Rainier Model 103 adiabatic demagnetization refrigerator (ADR) down to 50 mK. We add ~ 100 dB of attenuation distributed among different temperature stages to the input line³⁰. We shield the sample from stray magnetic fields with a high permeability can (Amuneal Cryoperm) surrounding the sample package. The output of the sample passes through one circulator to a high electron mobility transistor (HEMT) amplifier at the 4 K stage. Further amplification is used at room temperature.

A vector network analyzer (VNA) is used to measure the transmission through the sample. The Q_i of each resonator is extracted at different average circulating photon numbers $\langle n \rangle$ ranging from ~ 1 to $\sim 10^7$ using the diameter correction method³⁵ (DCM). $F\delta_{\text{TLS}}$ and the high-power internal quality factor Q_i^{HP} are calculated from⁸

$$F\delta_{\text{TLS}} \frac{\tanh(\frac{hf}{k_B T})}{\sqrt{1 + \frac{\langle n \rangle}{n_c}}} = \frac{1}{Q_i^{\text{HP}}} - \frac{1}{Q_i}, \quad (1)$$

where h is the Planck constant, f is the resonant frequency of the resonator, k_B is the Boltzmann constant, T is the temperature of the resonator, and n_c is the critical photon number that differentiates the high and low power regions. When $\langle n \rangle$ is large, the contribution to microwave loss from saturable TLSs approaches zero, so Q_i^{HP} gives a good estimate of the other sources of loss which mainly result from quasiparticles, trapped magnetic flux, radiation, and unsaturable TLSs.

Figure 5(a) shows a comparison of the $F\delta_{\text{TLS}}$ value among plasma passivated and untreated samples of both designs. Untreated resonators with the $3 \mu\text{m}$ center strip geometry have an average $F\delta_{\text{TLS}}$ of $(12.5 \pm 1.5) \cdot 10^{-7}$. This agrees with the result for untreated samples obtained in our previous study²⁹, which uses the same design but intrinsic Si (100) wafers instead of Si (111). In comparison, the passivated resonators have an average $F\delta_{\text{TLS}}$ of $(2.9 \pm 0.5) \cdot 10^{-7}$, which is ~ 4 times lower than the untreated value. Resonators with the $20 \mu\text{m}$ center strip geometry have an average $F\delta_{\text{TLS}}$ of $(4.6 \pm 1.0) \cdot 10^{-7}$ for untreated samples and $F\delta_{\text{TLS}}$ of $(1.0 \pm 0.3) \cdot 10^{-7}$ for passivated samples. Figure 5(b) shows the extracted Q_i^{HP} of the same resonators shown in Fig. 5(a). Resonators with the $3 \mu\text{m}$ center strip geometry show an increased Q_i^{HP} compared to untreated devices. We attribute this to a reduced TLS density in the regions of the sample that are too far from the resonators to be effectively saturated at high power. The Q_i^{HP} values of the resonators with the $20 \mu\text{m}$ center strip geometry are less uniform. We suspect that this could be due to their susceptibility to trapped vortices and radiation to lossy regions inside the package. The Q_i^{HP} values of our resonators are lower compared to other similar studies^{12,23}, which we attribute to specific details of the sample package^{33,36} and measurement setup.

To test the stability of the passivated samples over time, we allow some of the samples to age in an ambient environment for 45 days. Figure 5(a) indicates the change in $F\delta_{\text{TLS}}$ after this aging duration. We observe negligible change in $F\delta_{\text{TLS}}$ for the untreated devices, indicating that the oxide had already reached self-limited thickness before the first measurement. The passivated resonators exhibit increased $F\delta_{\text{TLS}}$ of varying degrees. In particular, two of the five passivated resonators maintained a significantly lower $F\delta_{\text{TLS}}$ compared to the untreated resonators, validating the stability of the passivated samples. Three of the passivated resonators, however, exhibited a significant increase in $F\delta_{\text{TLS}}$, which could be due to additional contamination of the resonators during storage. Visual inspection reveals significant residue and debris in the gap regions of CPWs for the resonators with significantly increased $F\delta_{\text{TLS}}$, indicating that the reduced performance could

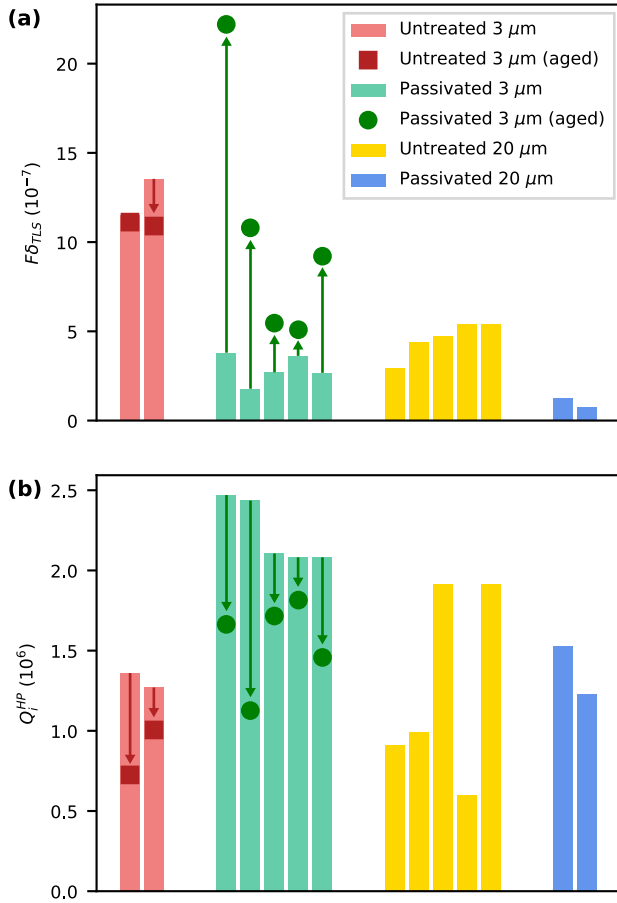


FIG. 5. **Microwave performance of passivated and untreated samples.** (a) Extracted $F\delta_{\text{TLS}}$ values among plasma passivated and untreated resonators with 3 μm and 20 μm center strip geometries. (b) Extracted Q_i^{HP} of the same resonators shown in (a).

be due to contamination during storage. In Fig. 5(b) we indicate the change in Q_i^{HP} for the aged devices. For all samples we observe a reduction in Q_i^{HP} after aging.

Our study demonstrates a recipe for passivation of Nb structures with nitrogen plasma which dopes the top 5 nm of the Nb surface with N atoms. These N atoms suppress the O concentration and therefore reduce the amount of TLS defects that induce microwave loss. The N and O populations are stable after 15 days of aging in ambient air according to XPS measurements. Cryogenic microwave measurements confirm that our passivation process reduces the microwave loss of CPW resonators of two different design geometries. Our process removes the stringent time sensitivity associated with the regrowth of NbO_x and allows for the incorporation of low microwave loss Nb structures into state-of-the-art quantum processors. Our process also creates a platform on which other sources of microwave loss can be further studied. Although T_c and XRD measurements suggest that our process creates a more disordered superconductor, which may increase the susceptibility to losses caused by quasiparticle and magnetic vor-

tices, these mechanisms do not yet dominate the microwave loss. While the side effect of suppressed superconductivity may be reduced by starting with Nb films with large grain size, the suppressed superconductivity may also be useful in producing low loss kinetic-inductance-based sensors^{37,38}. As Ta also has a superconducting nitride³⁹ and it is more refractory than Nb, our passivation process may also work in reducing the microwave loss of Ta.

ACKNOWLEDGMENTS

This research is supported by NSF Grant No. PHY-1752844 (CAREER), AFOSR MURI Grant No. FA9550-21-1-0202, and the John Templeton Foundation, Grant No. 61835. The authors acknowledge the use of facilities at the Institute of Materials Science and Engineering in Washington University.

DATA AVAILABILITY STATEMENT

The data that support the findings of this study are available from the corresponding author upon reasonable request.

- ¹F. Arute, K. Arya, R. Babbush, D. Bacon, J. C. Bardin, R. Barends, R. Biswas, S. Boixo, F. G. S. L. Brandao, D. A. Buell, B. Burkett, Y. Chen, Z. Chen, B. Chiaro, R. Collins, W. Courtney, A. Dunsworth, E. Farhi, B. Foxen, A. Fowler, C. Gidney, M. Giustina, R. Graff, K. Guerin, S. Habegger, M. P. Harrigan, M. J. Hartmann, A. Ho, M. Hoffmann, T. Huang, T. S. Humble, S. V. Isakov, E. Jeffrey, Z. Jiang, D. Kafri, K. Kechedzhi, J. Kelly, P. V. Klimov, S. Knysh, A. Korotkov, F. Kostritsa, D. Landhuis, M. Lindmark, E. Lucero, D. Lyakh, S. Mandrà, J. R. McClean, M. McEwen, A. Megrant, X. Mi, K. Michielsen, M. Mohseni, J. Mutus, O. Naaman, M. Neeley, C. Neill, M. Y. Niu, E. Ostby, A. Petukhov, J. C. Platt, C. Quintana, E. G. Rieffel, P. Roushan, N. C. Rubin, D. Sank, K. J. Satzinger, V. Smelyanskiy, K. J. Sung, M. D. Trevithick, A. Vainsencher, B. Villalonga, T. White, Z. J. Yao, P. Yeh, A. Zalcman, H. Neven, and J. M. Martinis, "Quantum supremacy using a programmable superconducting processor," *Nature* **574**, 505–510 (2019).
- ²P. Jurcevic, A. Javadi-Abhari, L. S. Bishop, I. Lauer, D. F. Bogorin, M. Brink, L. Capelluto, O. Günlük, T. Itoko, N. Kanazawa, A. Kandala, G. A. Keefe, K. Krsulich, W. Landers, E. P. Lewandowski, D. T. McClure, G. Nannicini, A. Narasgond, H. M. Nayfeh, E. Pritchett, M. B. Rothwell, S. Srinivasan, N. Sundaresan, C. Wang, K. X. Wei, C. J. Wood, J.-B. Yau, E. J. Zhang, O. E. Dial, J. M. Chow, and J. M. Gambetta, "Demonstration of quantum volume 64 on a superconducting quantum computing system," *Quantum Science and Technology* **6**, 025020 (2021).
- ³W. D. Oliver and P. B. Welander, "Materials in superconducting quantum bits," *MRS Bulletin* **38**, 816–825 (2013).
- ⁴C. E. Murray, "Material matters in superconducting qubits," (2021), arXiv:2106.05919 [quant-ph].
- ⁵B. Josephson, "Possible new effects in superconductive tunnelling," *Physics Letters* **1**, 251–253 (1962).
- ⁶P. W. Anderson and J. M. Rowell, "Probable observation of the josephson superconducting tunneling effect," *Phys. Rev. Lett.* **10**, 230–232 (1963).
- ⁷A. D. O'Connell, M. Ansmann, R. C. Bialczak, M. Hofheinz, N. Katz, E. Lucero, C. McKenney, M. Neeley, H. Wang, E. M. Weig, A. N. Cleland, and J. M. Martinis, "Microwave dielectric loss at single photon energies and millikelvin temperatures," *Applied Physics Letters* **92**, 112903 (2008), <https://doi.org/10.1063/1.2898887>.
- ⁸C. R. H. McRae, H. Wang, J. Gao, M. R. Vissers, T. Brecht, A. Dunsworth, D. P. Pappas, and J. Mutus, "Materials loss measurements using superconducting microwave resonators," *Review of Scientific Instruments* **91**, 091101 (2020), <https://doi.org/10.1063/5.0017378>.

- ⁹A. Nersisyan, S. Poletto, N. Alidoust, R. Manenti, R. Renzas, C.-V. Bui, K. Vu, T. Whyland, Y. Mohan, E. A. Sete, S. Stanwyck, A. Bestwick, and M. Reagor, "Manufacturing low dissipation superconducting quantum processors," in *2019 IEEE International Electron Devices Meeting (IEDM)* (2019) pp. 31.1.1–31.1.4.
- ¹⁰A. P. M. Place, L. V. H. Rodgers, P. Mundada, B. M. Smitham, M. Fitzpatrick, Z. Leng, A. Premkumar, J. Bryon, A. Vrajitoarea, S. Sussman, G. Cheng, T. Madhavan, H. K. Babla, X. H. Le, Y. Gang, B. Jäck, A. Gye-nis, N. Yao, R. J. Cava, N. P. de Leon, and A. A. Houck, "New material plat-form for superconducting transmon qubits with coherence times exceeding 0.3 milliseconds," *Nature Communications* **12**, 1779 (2021).
- ¹¹C. Müller, J. H. Cole, and J. Lisenfeld, "Towards understanding two-level-systems in amorphous solids: insights from quantum circuits," *Reports on Progress in Physics* **82**, 124501 (2019).
- ¹²M. V. P. Altoé, A. Banerjee, C. Berk, A. Hajr, A. Schwartzberg, C. Song, M. A. Ghadeer, S. Aloni, M. J. Elowson, J. M. Kreikebaum, E. K. Wong, S. Griffin, S. Rao, A. Weber-Bargioni, A. M. Minor, D. I. Santiago, S. Cabrini, I. Siddiqi, and D. F. Ogletree, "Localization and reduction of superconducting quantum coherent circuit losses," (2020), arXiv:2012.07604 [quant-ph].
- ¹³N. Cabrera and N. F. Mott, "Theory of the oxidation of metals," *Reports on Progress in Physics* **12**, 163–184 (1949).
- ¹⁴J. Verjauw, A. Potočnik, M. Mongillo, R. Acharya, F. Mohiyaddin, G. Simion, A. Pacco, T. Ivanov, D. Wan, A. Vanleenhove, L. Souriau, J. Jus-sot, A. Thiam, J. Swerts, X. Piao, S. Couet, M. Heyns, B. Govoreanu, and I. Radu, "Investigation of microwave loss induced by oxide regrowth in high-q niobium resonators," *Phys. Rev. Applied* **16**, 014018 (2021).
- ¹⁵K. Sokhey, S. Rai, and G. Lodha, "Oxidation studies of niobium thin films at room temperature by x-ray reflectivity," *Applied Surface Science* **257**, 222–226 (2010).
- ¹⁶K. Williams, K. Gupta, and M. Wasilik, "Etch rates for micromachining processing-part ii," *Journal of Microelectromechanical Systems* **12**, 761–778 (2003).
- ¹⁷L. Zhang, L. You, L. Ying, W. Peng, and Z. Wang, "Characterization of surface oxidation layers on ultrathin nbtin films," *Physica C: Superconductivity and its Applications* **545**, 1–4 (2018).
- ¹⁸M. R. Vissers, J. Gao, D. S. Wisbey, D. A. Hite, C. C. Tsuei, A. D. Cor-coles, M. Steffen, and D. P. Pappas, "Low loss superconducting titanium nitride coplanar waveguide resonators," *Applied Physics Letters* **97**, 232509 (2010), <https://doi.org/10.1063/1.3517252>.
- ¹⁹A. Melville, G. Calusine, W. Woods, K. Serniak, E. Golden, B. M. Niedzielski, D. K. Kim, A. Sevi, J. L. Yoder, E. A. Dauler, and W. D. Oliver, "Comparison of dielectric loss in titanium nitride and aluminum superconducting resonators," *Applied Physics Letters* **117**, 124004 (2020), <https://doi.org/10.1063/5.0021950>.
- ²⁰C. Berk, A. Banerjee, A. HAJR, J. M. Kreikebaum, V. Altoé, D. Santiago, D. F. Ogletree, and I. Siddiqi, "Improvement in superconducting resonator quality factor through surface passivation," *Bulletin of the American Physical Society* (2021).
- ²¹A. Grassellino, A. Romanenko, D. Sergatskov, O. Melnychuk, Y. Trenikhina, A. Crawford, A. Rowe, M. Wong, T. Khabiboulline, and F. Barkov, "Nitrogen and argon doping of niobium for superconducting radio frequency cavities: a pathway to highly efficient accelerating structures," *Superconductor Science and Technology* **26**, 102001 (2013).
- ²²G. D. L. Semione, A. D. Pandey, S. Tober, J. Pfrommer, A. Poulain, J. Drnc, G. Schütz, T. F. Keller, H. Noei, V. Vonk, B. Foster, and A. Stierle, "Niobium near-surface composition during nitrogen infusion relevant for superconducting radio-frequency cavities," *Phys. Rev. Accel. Beams* **22**, 103102 (2019).
- ²³A. Megrant, C. Neill, R. Barends, B. Chiaro, Y. Chen, L. Feigl, J. Kelly, E. Lucero, M. Mariantoni, P. J. J. O'Malley, D. Sank, A. Vainsencher, J. Wenner, T. C. White, Y. Yin, J. Zhao, C. J. Palmström, J. M. Martinis, and A. N. Cleland, "Planar superconducting resonators with internal qual-ity factors above one million," *Applied Physics Letters* **100**, 113510 (2012), <https://doi.org/10.1063/1.3693409>.
- ²⁴A. Premkumar, C. Weiland, S. Hwang, B. Jäck, A. P. M. Place, I. Waluyo, A. Hunt, V. Bisogni, J. Pellicciari, A. Barbour, M. S. Miller, P. Russo, F. Camino, K. Kisslinger, X. Tong, M. S. Hybertsen, A. A. Houck, and I. Jarrige, "Microscopic relaxation channels in materials for superconduct-ing qubits," *Communications Materials* **2**, 72 (2021).
- ²⁵C. Kopas, M. K. Murthy, C. Gregory, B. I. Mercado, D. R. Queen, B. Wagner, and N. Newman, "Characterization of the chemical and electrical properties of defects at the niobium-silicon interface," (2020), arXiv:2011.08359 [cond-mat.mtrl-sci].
- ²⁶Since Nb does not match to the lattice of Si (111) or Si (100), we expect similar results independent of wafer orientation.
- ²⁷A. V. Razinkin, E. Shalaeva, and M. V. Kuznetsov, "Photoelectron spec-troscopy and diffraction of nbx/nb(110) surface," *The Physics of Metals and Metallography* **106**, 56–66 (2008).
- ²⁸J. Halbritter, "On the oxidation and on the superconductivity of niobium," *Applied Physics A* **43**, 1–28 (1987).
- ²⁹D. Kowsari, K. Zheng, J. T. Monroe, N. J. Thobaben, X. Du, P. M. Harrington, E. A. Henriksen, D. S. Wisbey, and K. W. Murch, "Fabrication and surface treatment of electron-beam evaporated niobium for low-loss copla-nar waveguide resonators," *Applied Physics Letters* **119**, 132601 (2021), <https://doi.org/10.1063/5.0066441>.
- ³⁰D. S. Wisbey, M. R. Vissers, J. Gao, J. S. Kline, M. O. Sandberg, M. P. Weides, M. M. Paquette, S. Karki, J. Brewster, D. Alameri, I. Kuljanishvili, A. N. Caruso, and D. P. Pappas, "Dielectric loss of boron-based dielectrics on niobium resonators," *Journal of Low Temperature Physics* **195**, 474–486 (2019).
- ³¹C. Song, T. W. Heitmann, M. P. DeFeo, K. Yu, R. McDermott, M. Neeley, J. M. Martinis, and B. L. T. Plourde, "Microwave response of vortices in superconducting thin films of re and al," *Phys. Rev. B* **79**, 174512 (2009).
- ³²P. J. de Visser, J. J. A. Baselmans, S. J. C. Yates, P. Diener, A. Endo, and T. M. Klapwijk, "Microwave-induced excess quasipar-ticles in superconducting resonators measured through correlated con-ductivity fluctuations," *Applied Physics Letters* **100**, 162601 (2012), <https://doi.org/10.1063/1.4704151>.
- ³³S. Huang, B. Lienhard, G. Calusine, A. Vepsäläinen, J. Braumüller, D. K. Kim, A. J. Melville, B. M. Niedzielski, J. L. Yoder, B. Kannan, T. P. Or-lando, S. Gustavsson, and W. D. Oliver, "Microwave package design for superconducting quantum processors," *PRX Quantum* **2**, 020306 (2021).
- ³⁴I. Nsanzeza and B. L. T. Plourde, "Trapping a single vortex and reducing quasiparticles in a superconducting resonator," *Phys. Rev. Lett.* **113**, 117002 (2014).
- ³⁵M. S. Khalil, M. J. A. Stoutimore, F. C. Wellstood, and K. D. Osborn, "An analysis method for asymmetric resonator transmission applied to su-perconducting devices," *Journal of Applied Physics* **111**, 054510 (2012), <https://doi.org/10.1063/1.3692073>.
- ³⁶R. A. Matula, "Electrical resistivity of copper, gold, palladium, and silver," *Journal of Physical and Chemical Reference Data* **8**, 1147–1298 (1979), <https://doi.org/10.1063/1.555614>.
- ³⁷J. Zmuidzinas, "Superconducting microresonators: Physics and applica-tions," *Annual Review of Condensed Matter Physics* **3**, 169–214 (2012), <https://doi.org/10.1146/annurev-conmatphys-020911-125022>.
- ³⁸M. R. Vissers, J. Gao, M. Sandberg, S. M. Duff, D. S. Wisbey, K. D. Ir-win, and D. P. Pappas, "Proximity-coupled ti/tin multilayers for use in kinetic inductance detectors," *Applied Physics Letters* **102**, 232603 (2013), <https://doi.org/10.1063/1.4804286>.
- ³⁹N. P. Breznay, M. Tendulkar, L. Zhang, S.-C. Lee, and A. Kapitulnik, "Su-perconductor to weak-insulator transitions in disordered tantalum nitride films," *Phys. Rev. B* **96**, 134522 (2017).